Intel Serv Robotics (2016) 9:277–287
DOI 10.1007/s11370-016-0197-2

SPECIAL ISSUE

The design of a new remote manipulator for space operation using a 4-cable-driven thrusters-embedded configuration

Meng Li[1] · **Weizhong Guo**[1]

Received: 31 March 2015 / Accepted: 4 April 2016 / Published online: 20 April 2016

Abstract A new remote manipulator based on cable-driven parallel mechanism (CDPM) is designed for space long-distance operations (e.g. space capture/docking and other long-distance space activities) in this paper. By controlling the cables and thrusters which are equipped on the manipulator simultaneously, the new remote manipulator can achieve expected position, linear velocity, and angular velocity. The new manipulator has a larger controllable workspace compared with usual CDPMs. The structure and characteristics of this manipulator are discussed in this paper. The volume and characteristics of the workspace are also discussed. The influence of the distance on the static equilibrium is studied. The simulation results show that the workspace of this new manipulator is larger than usual CDPM's. The results also indicate that the cable forces and thruster vectors can completely constrain the manipulator and meet the requirements of space activities. The results of the simulation also show that the controllable workspace of the manipulator is not continuous at some regions. Hence, trajectory planning is necessary.

Keywords Space operation · Cable-driven remote manipulator · External thrusters · Static equilibrium · Workspace

1 Introduction

Over the past few decades, robots have played an increasingly important role in space activities and missions. The space robots (space remote manipulator system), such as Canadarm, Dextre, and ETS-VII [1], have been a crucial element in all space construction activities and other space missions. The space missions currently being planned by space agencies around the world, like Orbital Express mission of the U.S. Defence Advanced Research Project Agency (DARPA) [2] and the ConeXpress Orbital Life Extension Vehicle (CXOLEV) of Orbital Recovery [3], show an increase in the number of robots.

Manned space docking of space assembly, on-orbit servicing of failed or failing spacecraft, and remote operation of space maintenance are the main areas for the application of space robotics. Approach, posture adjustment and capture are the main common tasks of space activities. These tasks are usually conducted in a serial of remote manipulations and considered as the most risky space actives because the space robot and target not only have to match up at the right time and right position, but also have to be oriented correctly with respect to each other, with relative velocity and acceleration components near to zero. Some specific space robots have been developed in the past for these tasks: (1) Rigid body space robots Canadarm and Canadarm2 have been used in space activities for many years [4]. Dextre developed by Canada had been launched in 2007 and now is used to perform maintenance tasks. European Robotic Arm (ERA) [5] developed by European Space Agency (ESA) and JEMRMS [6] developed by Japanese Space Agency are also applied to constructing the International Space Station. ETS-VII involved the capture of a target satellite using a chaser satellite equipped with a robotic arm. The robotic capture was performed while the two satellites were still tied using the latching mechanism [7,8]. In the framework of this mission, future work is also discussed for a non-cooperative satellite [9]. NASA developed the first humanoid robot (Robonaut 2) for space tasks [10]. Other new rigid body space robots can be found in [11,12].

✉ Weizhong Guo
wzguo@sjtu.edu.cn

[1] School of Mechanical Engineering, Shanghai Jiao Tong University, Shanghai, China

(2) Tethered space robot

Basically, the space robotics mentioned above are rigid robotic arms equipped with a chaser satellite (or spacecraft). It must be noted that a risk assessment or collision probability exists in these developments. Recently, many researches paid more attention to Low-Impact Docking Systems. Because of the benefits of the cable/tether, the field of space tethers received much considerable attention in recent decades. The benefits of cable/tether compared to rigid robotics include the following features: (1) flexible and low impact. (2) Saving the mass and dimension of the manipulator. (3) Increasing effectiveness in terms of the area-time-product and (4) being reusable and returnable. Various conducting tether configurations have been studied and their de-orbiting performances have been assessed by several authors [13–15]. However, these researches about the remote manipulators are based on cables/tethers focused on in-plane manipulation (in-plane payload capture).

Long-distance operations based on cables/tethers for ground applications are very common, like object transportation to environments inaccessible by aerial robots [16,17] and boom [18]. But very few papers pay attention to the applications of on-orbit space operation. The boom docking system based on cables (tethers) is the leading approach for remote space operation (as shown in Fig. 1) [19]. Three or even more cable booms are engaged to have better control over the target. An on-orbit capture concept was proposed in [20] based on tether-net system. One other tether-net system was also proposed in [21].

For the special requirements of those space activities, the remote manipulators or space robots have three main characteristics: (1) a larger controllable workspace, (2) a smaller mounting space which is limited by the size of spaceship/space station and (3) a minimized number of thrusters.

In this work, we present a novel concept of long-distance space manipulator based on cable-driven parallel mechanism (CDPM). By controlling the cables/tethers and thrusters which are equipped on the manipulator, we can adjust the position and orientation of the manipulator.

Section 2 introduces the concept of the remote manipulator and presents the mechanics of this remote manipulator. Section 3 presents the critical phases and mechanism of a typical space mission which completed by the new manipulator. Section 4 studies the influence of the distance between the manipulator and spaceship on the workspace. Section 5 concludes our work.

2 The configuration and mechanics

2.1 The configuration of the remote manipulator

Normally, the space manipulators are activated by chaser satellites. The common chaser satellites have such characteristics as heavy weight and large size since the satellites are always equipped with many thrusters and a large amount of fuel. In the design of the new space manipulator, we replace some thrusters with cables or tethers, and adjust the

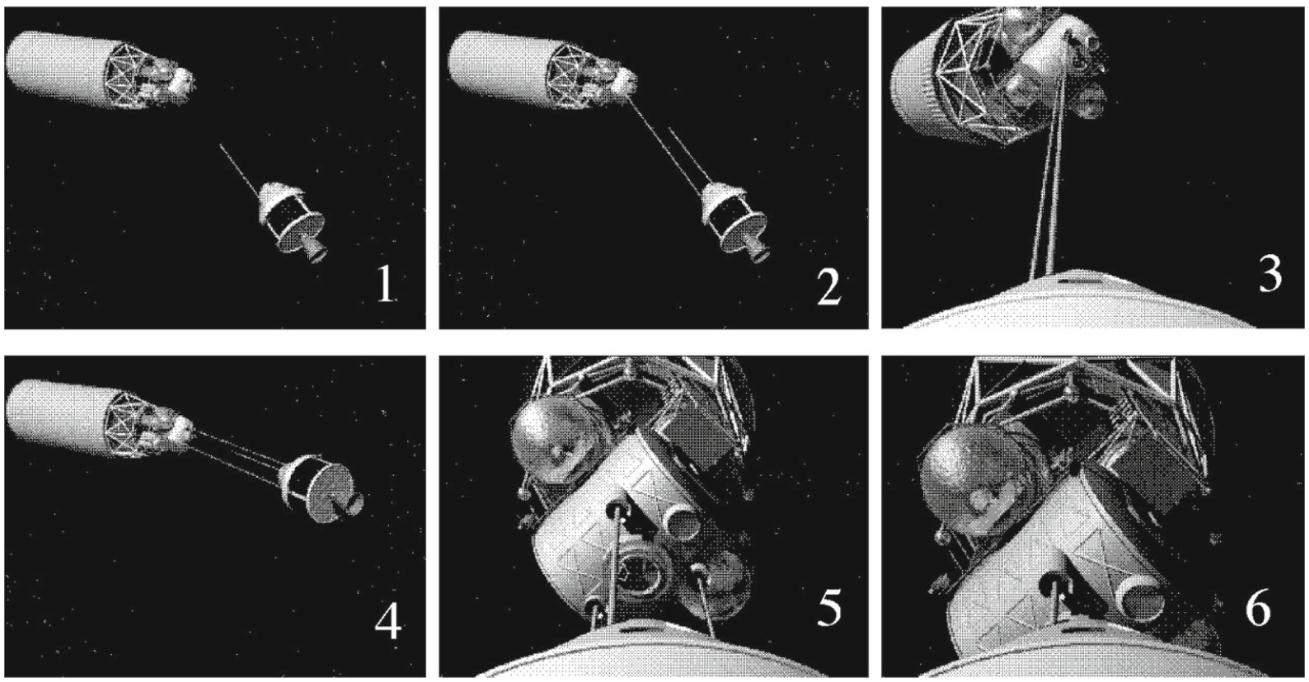

Fig. 1 The boom docking system (adapted from Ref. [19])

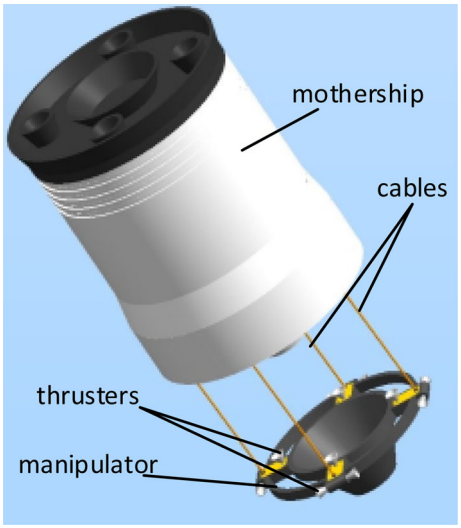

Fig. 2 The design and configuration of the new manipulator

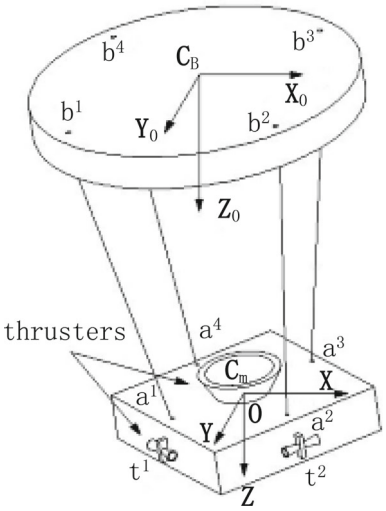

Fig. 3 The coordinate systems

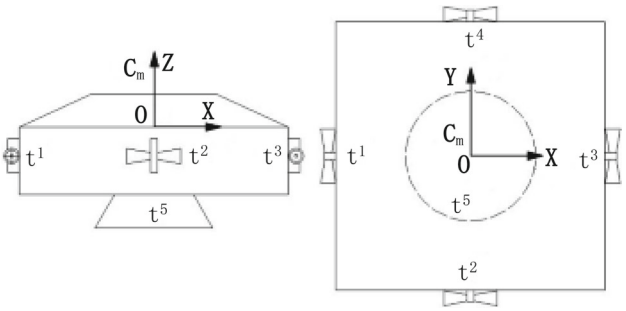

Fig. 4 The placement position of the thrusters

position and orientation of the manipulator by controlling cables/tethers and thrusters simultaneously. Instead of fuel, the solar cells provide energy for the motors of the manipulator. Thus, the mass and size of the manipulator can be significantly reduced to a minimum level.

Usually, a fully constrained CDPM robot requires $(n+1)$ (n is the DOFs of the end-effector) cables to fully constrain the end-effector (moving manipulator) [22]. The robot needs a large overhead space to constrain all DOFs [23]. The under-constrained CDPM does not require large overhead space. But the manipulator of under-constrained CDPM preserves $(6-n)$ DOFs since only n ($n < 6$) geometrical restrains are enforced, which is pointed in [22]. So we introduce external thrusters to constrain the DOFs that the manipulator preserved. The proposed novel manipulator is illustrated in Fig. 2. The motors and power of the manipulator are mounted on spaceship (or space station). The major characteristic of the under-constrained CDPMs consists in the intrinsic coupling between kinematics and statics (or dynamics). Hence, geometrico-closure and static-equilibrium must be simultaneously solved. Furthermore, because the actual pose of the platform depends on the applied work load and external force, investigating equilibrium stability is necessary.

2.2 Problem formulation

Similar to the analysis of usual under-constrained CDPM, the spaceship (space station) can be regarded as the base of CDPM, and the manipulator can be treated as the moving end-effector. A base coordinate system $\boldsymbol{C_B}$ is to be placed on the spaceship (or space station). The base points of the manipulator $b_B^1, b_B^2, b_B^3, \ldots, b_B^n$ are all fixed on the spaceship (space station) and contained within the same plane ($Z_0 = 0$) relative to base coordinate system $\boldsymbol{C_B}$. A moving coordinate system $\boldsymbol{C_M}$ attached at $\mathbf{O}$ which is the center of the manipulator. The moving points of the manipulator $a_M^1, a_M^2, \ldots, a_M^n$ are all fixed on the manipulator and contained within the same plane. We placed two pairs of jet-thrusters on the manipulator (as shown in Fig. 3). One pair of jet-thrusters is parallel to the x-axis of coordinate system $\boldsymbol{C_M}$ and the other pair of jet-thrusters is parallel to the y-axis of coordinate system $\boldsymbol{C_M}$. One thruster is to be placed at the bottom of the moving platform (as shown in Fig. 4). Obviously the external thrusters can be placed in other position, and the placement of the external thrusters influences the workspace and controllability of the manipulator directly. We will discuss this problem in our later works.

The origin of moving coordinate system $\boldsymbol{C_M}$ with respect to base coordinate system $\boldsymbol{C_B}$ is represented by the position vector $\mathbf{r} = [x_O\ y_o\ z_o]^T$, while the orientation of moving coordinate system $\boldsymbol{C_M}$ with respect to base coordinate system $\boldsymbol{C_B}$ is represented by the rotation matrix $\mathbf{R} \in SO(3)$. Vectors $\boldsymbol{a_M^i}$ ($i = 1, 2, \ldots, n$) represent the position vectors of the cable attachment points a_M^i ($i = 1, 2, \ldots, n$) with respect to coordinate $\boldsymbol{C_M}$. Vectors $\boldsymbol{b_B^i}$ ($i = 1, 2, \ldots, n$) denote the location of the cable exit points at the base coordinate $\boldsymbol{C_B}$.

Vectors $\boldsymbol{t}_{\boldsymbol{M}}^{i}$ $(i = 1, \ldots 5)$ represent the position vectors of the thruster attachment points t_M^i $(i = 1, \ldots 5)$ with respect to coordinate $\boldsymbol{C_M}$. $\boldsymbol{f_e}$ and $\boldsymbol{m_e}$ are desired force and moment, respectively.

The homogeneous transformation matrix describing the pose of the manipulator is given by

$$A = \begin{bmatrix} & x_o \\ \boldsymbol{R}\,(\gamma, \theta, \varphi) & y_o \\ & z_o \\ \mathbf{0} & 1 \end{bmatrix} \tag{1}$$

Note that the rotation matrix $\mathbf{R}$ follows the $X_0 - Y_0 - Z_0$ fixed-angle parameterization for $\{\gamma, \theta, \varphi\}$.

The wrenches that the cables imposed on the manipulator can be expressed as the following form after normalization:

$$\boldsymbol{w}_i^c = \frac{1}{l_i}\begin{bmatrix} \boldsymbol{b}_{\boldsymbol{B}}^{i} - \mathbf{R}\boldsymbol{a}_{\boldsymbol{M}}^{i} - \mathbf{r} \\ \boldsymbol{a}_{\boldsymbol{M}}^{i} \times \left(\boldsymbol{b}_{\boldsymbol{B}}^{i} - \mathbf{R}\boldsymbol{a}_{\boldsymbol{M}}^{i} - \mathbf{r}\right) \end{bmatrix} (i = 1,\ 2,\ 3,\ 4) \tag{2}$$

The wrenches that the external thrusters imposed on the manipulator take the following form:

$$\boldsymbol{w}_i^t = \begin{bmatrix} \boldsymbol{Re}_1 \\ \boldsymbol{Rt}_{\boldsymbol{M}}^{i} \times \boldsymbol{Re}_1 \end{bmatrix} \quad (i = 1,\ 3) \tag{3}$$

$$\boldsymbol{w}_i^t = \begin{bmatrix} \boldsymbol{Re}_2 \\ \boldsymbol{Rt}_{\boldsymbol{M}}^{i} \times \boldsymbol{Re}_2 \end{bmatrix} \quad (i = 2, 4) \tag{4}$$

$$\boldsymbol{w}_i^t = \begin{bmatrix} \boldsymbol{Re}_3 \\ \mathbf{0} \times \boldsymbol{Re}_3 \end{bmatrix} \quad (i = 5), \tag{5}$$

where $\boldsymbol{e}_1 = [1, 0, 0]^T$, $\boldsymbol{e}_2 = [0, 1, 0]^T$ and $\boldsymbol{e}_3 = [0, 0, 1]^T$.

2.3 Cooperative manipulation

The analysis for n-cables-5-thruster manipulator in this paper is an illustration for the design concept of the remote manipulator. We will make the following simplifying assumptions for this case:

(1) The manipulator is a homogeneous, planar object and the center of mass lies in the plane of the three pivot point.
(2) The mass of the target is sufficiently small that the manipulator is able to move the object.
(3) The target does not need to flip during manipulation, restricting the orientation to $|\gamma| < \frac{\pi}{2}$, $|\theta| < \frac{\pi}{2}$, and $|\varphi| < \frac{\pi}{2}$ (γ, θ, φ are rotation angles about X, Y, and Z axes, respectively).

The thruster can only provide force along the direction of the thrust vector, so we can deal with the thruster as a kind of special cable which can provide positive and negative cable force. And the general static equilibrium can be expressed as

$$\mathbf{W}_{des} = \mathbf{A}_{des} \cdot \boldsymbol{\lambda}, \tag{6}$$

where $\mathbf{W}_{des} = -\left[\boldsymbol{f_e}\ \boldsymbol{m_e}\right]^T$ is the resultant force and wrench that the cables and thrusters acting on the manipulator. $\mathbf{A}_{des} = \left[\boldsymbol{w}_1^c\ \ldots\ \boldsymbol{w}_n^c\ \boldsymbol{w}_1^t\ \ldots\ \boldsymbol{w}_5^t\right]$ is the wrench matrix associated with the driving cables and thrusters, $\boldsymbol{\lambda} = \left[\lambda_1\ \ldots\ \lambda_i\ \ldots\ \lambda_{n+5}\right]^T$ is the cable tension and thruster thrust vector, and λ_i $(i = 1,\ 2,\ \ldots,\ n) \geq 0$.

3 Phases and mechanism of a typical space mission using the cable-driven thruster-embedded platform

A typical space mission is conducted in a series of operations of manipulator. Some of operations such as rendezvous and docking are performed by the chaser satellite or spacecraft, while others such as operation and service are performed by a robotic arm or tool of the chaser satellite or spacecraft. The normal phases of a typical space mission which is completed by common space robots have been discussed a lot in many works [24–26]. In this paragraph, we will describe the normal phases of a typical space mission by using the new remote manipulator and deduce the algorithms to generate the motion for the manipulator.

(1) Drift orbit of the spaceship

First, the spaceship needs to enter the same orbit as the target. This phase is called drift orbit. In this phase, the spaceship is usually within a distance of 5–10 km of the target. Action in this phase includes acquiring the information of the target and achieving the necessary position and velocity with respect to the target. Actions and operations in this phase are mainly completed by the spaceship, as seen in Fig. 5.

(2) Discharge of the remote manipulator

After the spaceship completed its drift orbit phase, the spaceship discharges the remote manipulator, as seen in Fig. 6. The remote manipulator is mainly guided and navigated by the absolute navigation aids. In this phase, the

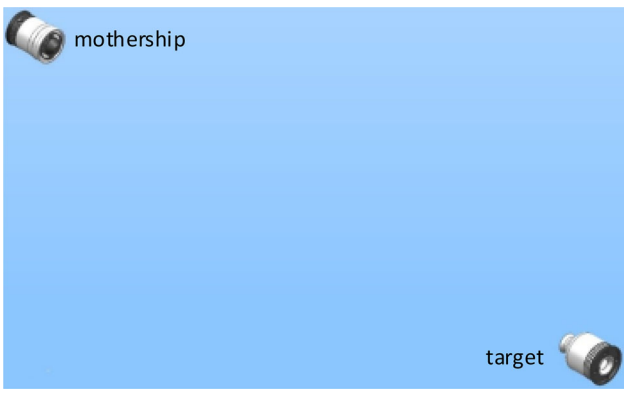

Fig. 5 Drift orbit of the spaceship

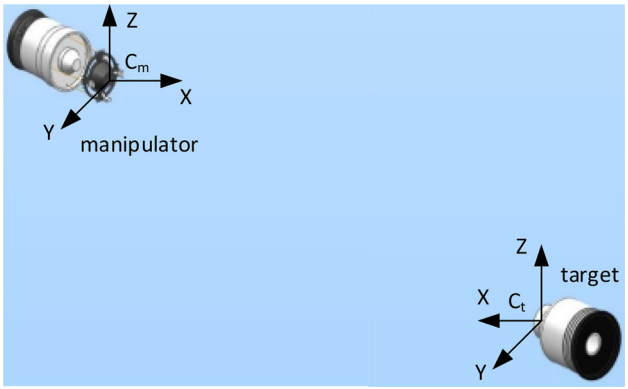

Fig. 6 Discharge of the remote manipulator and long-range rendezvous

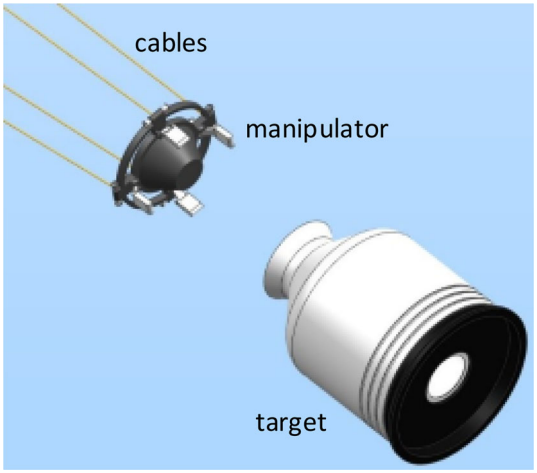

Fig. 7 Short-range rendezvous

attitude and velocity match between the manipulator and target is not a very important factor. Operations in this phase are performed by the thrusters.

(3) Long-range rendezvous

In this phase, the manipulator had discharged from the spaceship, and usually is within a distance of 300 m to 5 km of the target (as in Fig. 6 shown). Actions in this phase include acquiring and updating the information of the target, achieving the necessary position, velocity, and angular velocity with respect to the target for the subsequent short-range rendezvous. But similar to the phase of discharge, the attitude and velocity match between the manipulator and target is not a critical factor.

Based on the pose of the target frame $\boldsymbol{C_T}$ (see Fig. 6), a Cartesian acceleration vector is generated in the base frame $\boldsymbol{C_B}$ to progressively reduce the distance between the manipulator and target. The translation part of the long-Range can be modeled as

$$\ddot{\boldsymbol{d}}_{des} = \boldsymbol{f}_{\boldsymbol{des}}/m, \tag{7}$$

where $\ddot{\boldsymbol{d}}_{des}$ is the desired acceleration, $\boldsymbol{d}_{des}$ is the desired translation distance, $\boldsymbol{f}_{\boldsymbol{des}}$ is the resultant force (desired wrench), and m is the mass of the manipulator.

(4) Short-range rendezvous

The short-range rendezvous starts when the manipulator gets within 300 m of the target. This phase is active for distance from 300 m to several meters (as Fig. 7 shown). In this phase, the manipulator has to control not only the distance but also the relative attitude with respect to the target. The operation has to be controlled via sensing the relative position, attitude, and velocities of the target directly. Owing to the limitation of cables/ tethers, the trajectory of the manipulator must be restricted. In this phase, the adjustment of manipulator is completed by the thrusters and cables. The desired distance between the manipulator and target is controlled by the translational degrees of freedom that move the manipulator forward and backward. The translational motion can be computed from

$$\boldsymbol{d}_{des} = \boldsymbol{R_M r_M} - \boldsymbol{R_T r_T}, \tag{8}$$

where $\boldsymbol{R_M}$ and $\boldsymbol{R_T}$ are the rotation matrices representing the orientation of the manipulator frame $\boldsymbol{C_M}$, and the target frame $\boldsymbol{C_T}$ with respect to the base frame $\boldsymbol{C_B}$, respectively, $\boldsymbol{r_M}$ is the position of the manipulator frame expressed in the base frame, and $\boldsymbol{r_T}$ is the position of the target relative to the base frame. The attitude adjustment of the manipulator in this phase uses two rotational degree of freedom and is generated using

$$\boldsymbol{R}\,(\gamma)\,\boldsymbol{R}\,(\theta) = \boldsymbol{R_M^{-1} R_T}, \tag{9}$$

where γ, θ are rotation angles of the manipulator.

(5) Attitude adjustment and station keeping

After completing the phase of short-range rendezvous, the manipulator orients itself toward the target. The goal of this phase is to position the target in the center of the workspace of capture tool. During this phase, the manipulator is in very close proximity of the target such that the target is within the reach of the capture tool or arm (as in Fig. 8 shown). In order to avoid any collisions, the manipulator has to ensure that it is in a safe trajectory and attitude before attempting any capture operations. Actions of the manipulator in this phase must be strictly controlled by the thrusters and cables. If the manipulator may damage the target, the cables can drawback the manipulator and adjust its attitude or position in a safety distance.

(6) Capture

This phase is the core step of the mission. The operation in this phase involves touching between the manipulator and target, so it requires a timely cooperation of the control systems in both the manipulator and the target. In this phase, as shown

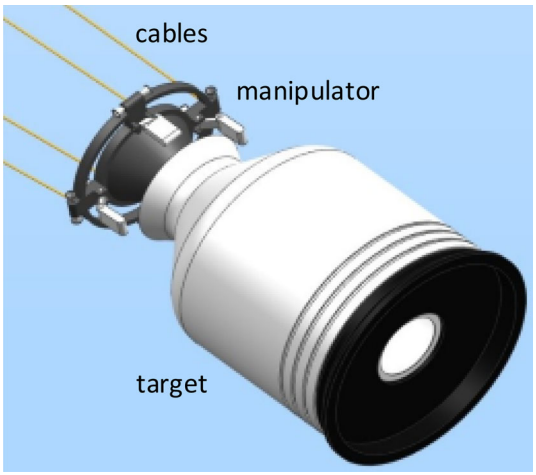

Fig. 8 Attitude adjustment and station keeping

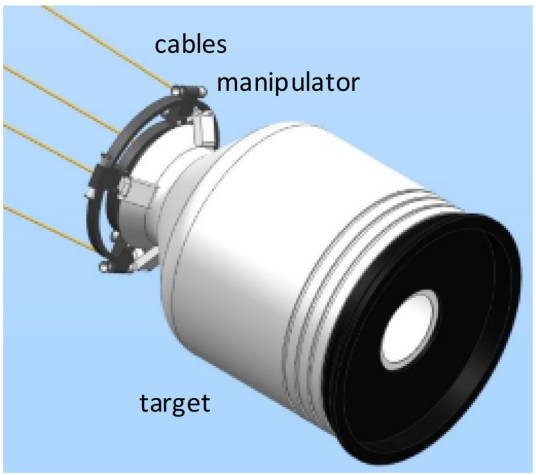

Fig. 9 Capture

in Fig. 9, the manipulator's robotic arm or tool approaches the target and grasps it. During capture, the manipulator makes a final closing and physical contact with the target through a docking interface. As a result, the manipulator and target are rigidly connected together. After capture, the motion of the target is completely controlled by the manipulator, and the subsequent operation starts.

(7) Returning

In the returning phase, the spaceship pulls back the cables and drives the target flying toward the spaceship. When the target is in a very close proximity to the spaceship, the manipulator starts to control its velocity and attitude (as shown in Fig. 10). After the cables are totally driven back, the manipulator will be fixed at the spaceship again.

3.1 Equilibrium configuration and cable length

Controlling the length of the cables/tethers is an important task for the cable-thruster manipulator. First, the cable length

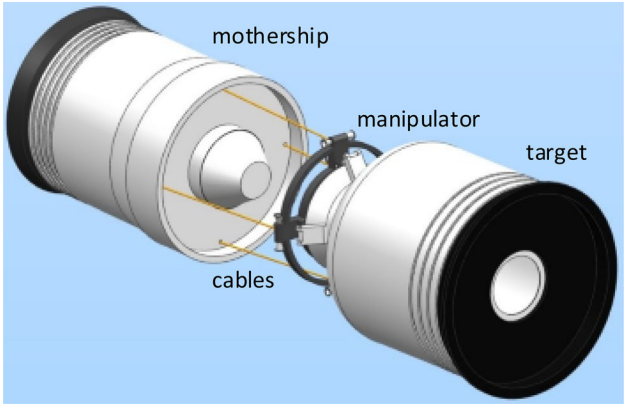

Fig. 10 Returning

is elongated or shortened to meet the requirements of the manipulation. Second, the cables must be in tension during the manipulation to prevent twine.

If all cables are in tension, there are four geometrical constraints imposed on the manipulator:

$$l_i^2 = \left\| \boldsymbol{a}^i - \boldsymbol{b}^i \right\|^2 \; i = 1 \ldots 4 \tag{10}$$

For the given position $\mathbf{r} = [x_O \; y_o \; z_o]^T$ and orientation $\boldsymbol{R}\,(\gamma, \theta, \varphi)$ of the manipulator, the cable length should be:

$$l_i^2 = \left\| \boldsymbol{b}^i - \boldsymbol{R}\,(\gamma, \theta, \varphi)\, \boldsymbol{a}^i + \mathbf{r} \right\| \; (i = 1, 2, \ldots, 4) \tag{11}$$

Finding the equilibrium configuration is also an important task to ensure that the manipulator is under control at current position and orientation. The method to solve the equilibrium configuration problem is similar to the method in [27]. Because the orientation and position of the manipulator are assigned, each column vectors $\boldsymbol{w}_i^c \; (i = 1, 2, \ldots, n)$ and $\boldsymbol{w}_i^t \; (i = 1, 2, 3, 4, 5)$ of $\mathbf{A}_{des}$ can be got from Eqs. (2)–(5). The equilibrium configuration can be achieved if and only if there exists at least one set of cable tension vectors that satisfies $(\lambda_i \; (i = 1, 2, \ldots, n) \geq 0)$. We can get the cable tension vectors as follows:

Step. 1 Choose a set of k vectors ($k \leq n+5$, and k depends on the degree of the manipulation) from the column vectors of $\mathbf{A}_{des}$. Use the k vectors to form an $k \times k$ matrix G.

Step. 2 Ensure that rank(G) = k.

Step. 3 Determine vector λ_i as follows:

$$\boldsymbol{\lambda} = \mathbf{G}^{-1}\mathbf{W}_{des} \tag{12}$$

Step. 4 if $\lambda_i \; (i = 1, 2, \ldots, n) \geq 0$ and $\sum \lambda_i \neq 0 (I = 1, 2, \ldots, n+5)$, the configuration satisfies the

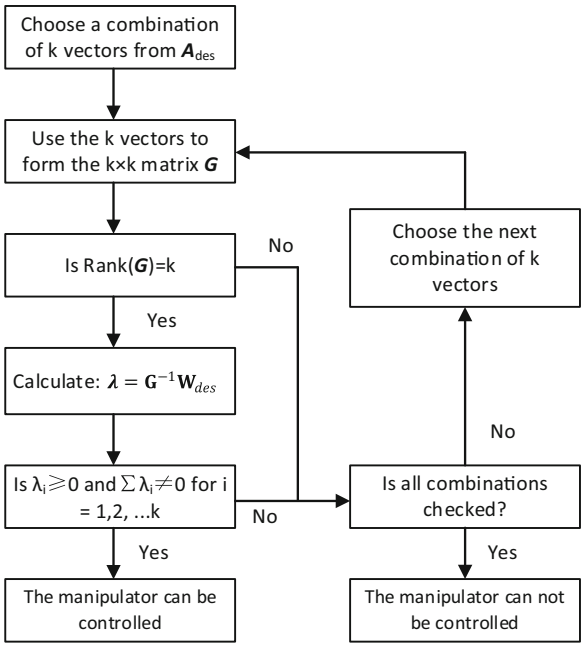

Fig. 11 Flow chart of the equilibrium configuration analysis algorithm

force-closure condition, and the manipulator can be controlled by the cables and thrusters.

The procedures are shown in Fig. 11.

3.2 Workspace and performance index

The static equilibrium can be used to find the cable forces and thruster forces which drive the manipulator to achieve the desired position and orientation. Suppose the resultant force and wrench is:

$$\mathbf{W}_{des} = [F_1 \ F_2 \ F_3 \ M_1 \ M_2 \ M_3]^T \tag{13}$$

The workspace of the remote manipulator will be characterized by the set of points where the center of mass of the manipulator can be positioned while all cables are in tension. A pose is in the workspace where there exists at least one set of positive cable tension that achieves static equilibrium while resisting the desired wrench $\mathbf{W}_{des}$.

The performance indexes of the manipulator indicate the subspaces of the workspace in which the manipulator performs better. This problem can be solved by checking the condition number of $\mathbf{A}_{des}$ or $\mathbf{A}_{des}^T$. The condition number κ is defined as

$$\kappa\left(\mathbf{A}_{des}\right) \equiv \frac{\sigma_1}{\sigma_s}, \tag{14}$$

and it is the ratio of the largest singular value σ_1 to the smallest singular value σ_s. The singular value is the square root of the eigenvalues of $\mathbf{A}_{des}\mathbf{A}_{des}^T$ and $\mathbf{A}_{des}^T\mathbf{A}_{des}$. The condition number ranges from:

$$1 \leq \kappa \leq \infty \tag{15}$$

The matrix $\mathbf{A}_{des}$ is well-conditioned when the condition number approaches 1, and this means the manipulator is far from singularities and easy to operate.

4 Case studies and simulation results

Based on the design configuration and algorithm presented above, an analysis of the new remote manipulator is performed. The configuration of the remote manipulator is as shown in Figs. 2 and 3. A program is created for the workspace analysis. The simulation results are presented in this section. The parameters include the connection points of the base, the moving platform, and the thruster (as shown in Table 1). Due to the lengthy computational time, the step size was fixed as 1, the search for possible workspace volume was confined to the region of $(-50 \leqslant x_O \leqslant 50, \ -50 \leqslant y_O \leqslant 50, \leqslant z_O \leqslant 1000)$. Once the parameters of the manipulator are selected, the program checks every point in the volume to see if the cables and the thrusters yield tensions and forces when the manipulator is positioned at each point of the possible workspace (according to actual condition, we limit the cable force and thrust force in $[0, 1000N]$).

4.1 Influence of the distance on the reachable workspace volume

Because the special configuration of the manipulator, the distance between the manipulator and spaceship plays a crucial role on the equilibrium capability of the manipulator. With the intention to assess the influence of the distance on the equilibrium capability, we performed several computational simulations. In the first scenario, we assume the manipulator needs to equilibrate a desired translational force $\mathbf{W}_{des}^1 = [F_1 \ F_2 \ F_3 \ 0 \ 0 \ 0]^T$. Suppose the orientation of the manipulator is $\gamma = 0, \theta = 0$ and $\varphi = 0$. The relationship between reachable workspace and distance is shown in Fig. 12. From the plots it can be observed that the manipulator presents a good performance and can equilibrate the desired force $\mathbf{W}_{des}^1$ easily in current orientation. The distance between manipulator and spaceship has limited effect on the translational performance of the manipulator.

In the second scenario, we assume that a moment $\mathbf{W}_{des}^2 = [0 \ 0 \ 0 \ M_1 \ 0 \ 0]^T$ acting on the manipulator. The initial posture of the manipulator is $\gamma = 0, \theta = 0$ and $\varphi = 0$. The result is as shown in Fig. 13. In Fig. 13, it can be observed that the distance between the manipulator and spaceship has significant influence on the volume of the reachable workspace.

Table 1 The parameters of the remote manipulator

Connect points	Unit (mm)	Connect points	Unit (mm)
a^1	[40, 60, −57.5]	b^4	[−130, −138.5, −57.5]
a^2	[−40, 60, −57.5]	t^1	[0, 60, 0]
a^3	[40, −60, −57.5]	t^2	[0, −60, 0]
a^4	[−40, −60, −57.5]	t^3	[40, 0, 0]
b^1	[−130, 138.5, −57.5]	t^4	[−40, 0, 0]
b^2	[50, 138.5, −57.5]	t^5	[0, 0, −57.5]
b^3	[50, −138.5, −57.5]		

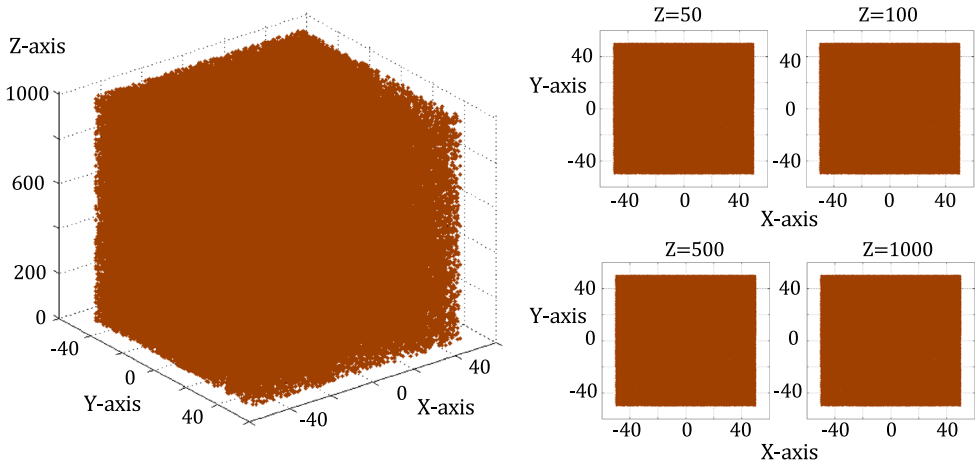

Fig. 12 The volume of the reachable workspace versus the distance ($\mathbf{W}_{des} = \mathbf{W}^1_{des}$)

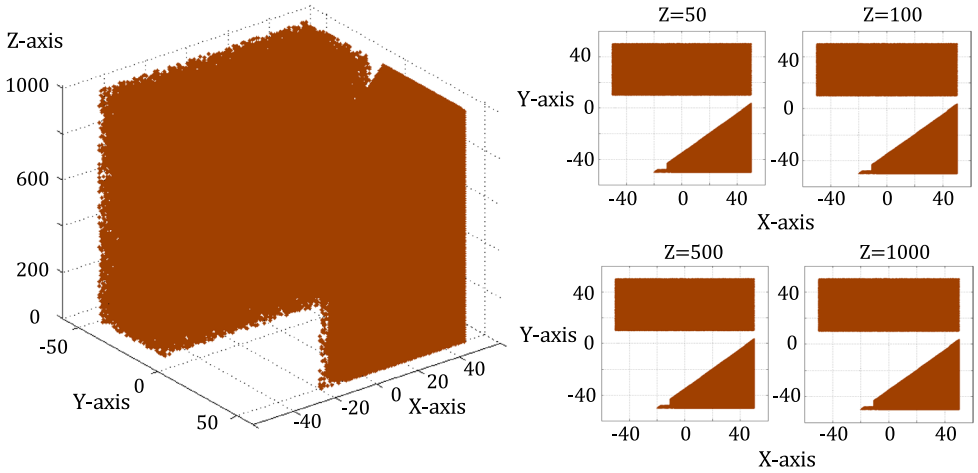

Fig. 13 The volume of the reachable workspace versus the distance ($\mathbf{W}_{des} = \mathbf{W}^2_{des}$)

The manipulator can equilibrate the desired moment $\mathbf{W}^2_{des}$ in some areas, but not all. Apparently, the distribution of the workspace is not continuous.

4.2 Influence of the distance on the dexterous workspace

Dexterous workspace is an important issue in the process of design of robot. This property indicates the global characteristics with respect to manipulability of the robot and is based on its kinematics and geometry. In order to study the influence of the distance between manipulator and spaceship on the dexterous workspace, a computational simulation is carried out by using the 4-cable-driven remote manipulator.

In order to generate the dexterous workspace, we suppose the manipulator is fixed at a certain position and divide the three-dimensional $\gamma - \theta - \varphi$ dexterous workspace into a series of subworkspaces. Then a numerical searching method based on the inverse kinematics is adopted to determine the value of the subworkspaces. Because there are three angular variables, some simplifications are made with the purpose to keep the analysis simple. Thus, we restrict the angular variable φ to zero. Furthermore, in the simulation performed, the position component of z-axis is the only position vari-

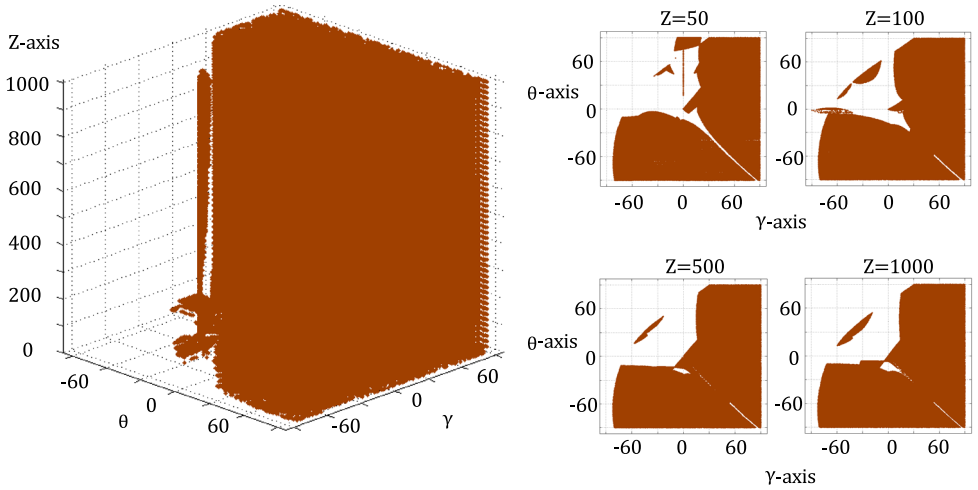

Fig. 14 The volume of the dexterous workspace versus the distance ($\mathbf{W}_{des} = \mathbf{W}^1_{des}$)

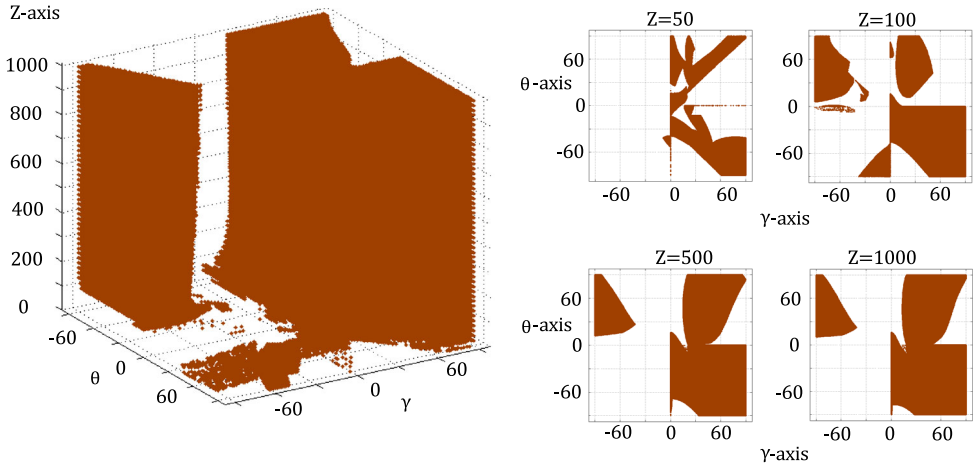

Fig. 15 The volume of the dexterous workspace versus the distance ($\mathbf{W}_{des} = \mathbf{W}^2_{des}$)

able which is considered. Hence, the position components of x-axis and y-axis are restricted to ($x = 0, y = 0$). Same as the reachable workspace analysis, two sets of wrenches are considered. In the first scenario, we assume that the manipulator needs to equilibrate a desired force $\mathbf{W}^1_{des} = [F_1\ F_2\ F_3\ 0\ 0\ 0]^T$. Figure 14 is the result of the dexterous workspaces with respect to different z-axis position. By analyzing Fig. 14, it can be observed that the distance has limited effect on the rotational performance of the manipulator. As the manipulator moves from $z = 10$ to $z = 1000$, the volume of the dexterous workspace has changed very little. In most areas of the workspace, the manipulator can equilibrate the desired force. In the results of Fig. 14, a significant characteristic can be observed that there are many singularities exist inside of the dexterous workspace. The distribution of the workspace is not continuous in some peculiar areas.

In the second scenario, we assume that the cables and thrusters need to supply a moment $\mathbf{W}^1_{des} = -[0\,0\,0\,M_1\,0\,0]^T$ on the manipulator which drives the manipulator to achieve the desired posture. The influence of the distance on the dexterous workspace can be seen in Fig. 15. From Fig. 15, it can be observed that the volume of the dexterous workspace increases as the manipulator moves from $z = 0$ to $z = 1000$. The manipulator can equilibrate the moment $\mathbf{W}^1_{des}$ in some peculiar subspaces, especially when $z \geq 100$. By analyzing Figs. 14 and 15, we can know that the dexterous workspace of the manipulator is not continuous.

In this section, we present an analysis of the influence of the distance between manipulator and spaceship on the volume of reachable workspace and dexterous workspace. These studies can evaluate the equilibrium stability of the new remote manipulator. The results show that the manipulator has excellent translational capability and rotational capability about z-axis. But the plots of the result also indicate that the manipulator still preserves some DOFs in some subregions of the workspace.

4.3 Performance indexes

The performance indexes with respect to the position of the remote manipulator are given in this section. After the remote manipulator moved through each point in the workspace the translational performance index can be calculated for the entire workspace. The translational performance index

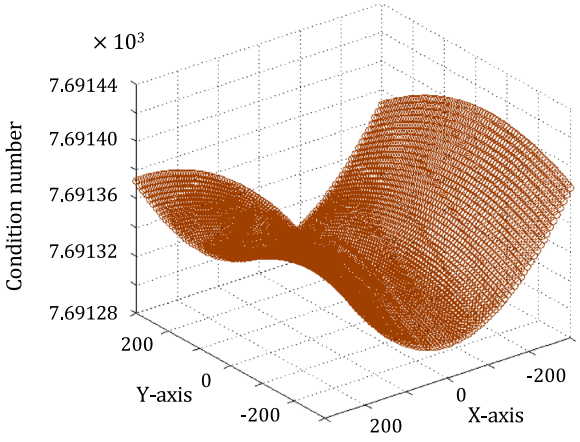

Fig. 16 Condition number κ versus x and y

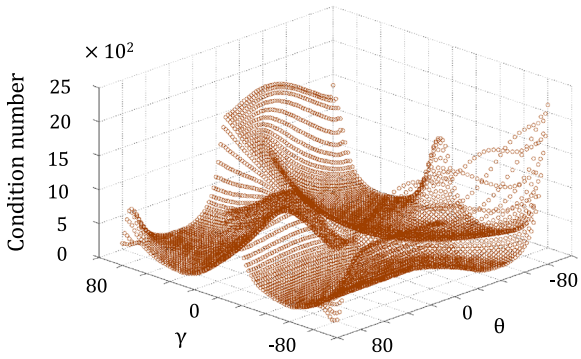

Fig. 17 Condition number κ versus γ and θ

is displayed in Fig. 16. From Fig. 16, it can be observed that the condition number increases as the manipulator moves from the center of x-y plane to the border of x-y plane. The manipulator has a better performance around the center of x-y plane. With the similar method, after the manipulator rotated through each angle at a certain position, the rotational performance index at this point can be calculated for the entire dexterous workspace. The result of the performance index is displayed in Fig. 17. By analyzing Fig. 17, it can be observed that the rotational performance index increases as the manipulator rotates itself from orientation $\gamma = 0°, \theta = 0°$ to orientation $\gamma = 60°, \theta = 60°$. Hence, the manipulator presents a superior performance around the orientation $\gamma = 0°, \theta = 0°$.

5 Conclusions

In this paper, we present a new design of remote manipulator based on the CDPM for space activities. In the design of the new space manipulator, we replace some thrusters of usual space manipulators with cables or tethers and adjust the manipulator by controlling the cables/tethers and thrusters simultaneously. Because the new remote manipulator is equipped with less thrusters and carries less amount of fuel, the mass and size of the remote manipulator can be significantly reduced to a minimum level. The critical phases of a typical space mission completed by the new remote manipulator is also presented in this paper. Mechanics of the manipulation, including the cooperative manipulation problem, equilibrium configuration problem and workspace, are also be considered in this paper.

As far as the feasibility of the new remote manipulator is concerned, a 4-CDPM with five external thrusters is taken as an example for the analysis of the new remote manipulator. The influence of the distance between manipulator and spaceship on the equilibrium capability of the manipulator is studied. The volume of the reachable workspace and dexterous workspace are studied too. The simulation results show that the manipulator has excellent translational capability and rotational capability about z-axis. With appropriate placement of external thrusters, the new remote manipulator can keep static equilibrium in workspace. The distance between the manipulator and spaceship has limited effect on the performance of the manipulator. But the results also indicate that the manipulator preserves some extra DOFs in some subregions of the workspace. In these subregions, the posture of the manipulator depends on the work load and external force. The plots of the simulations show that there are many singularities in the workspace. Hence, trajectory planning is necessary.

References

1. Kasai T, Oda M, Suzuki T (1999) Results of the ETS-7 Mission-Rendezvous docking and space robotics experiments. In: Artificial Intelligence, Robotics and Automation in Space, p 299
2. Whelan DA, Adler EA, Wilson III SB, Roesler Jr GM (2000) Darpa orbital express program: effecting a revolution in space-based systems. In: International Symposium on Optical Science and Technology, pp 48–56
3. Wingo DR (2004) Orbital recovery's responsive commercial space tug for life extension missions. In: AIAA 2nd Responsive Space Conference, Los Angeles
4. Stieber ME, Sachdev S, Lymer J (2000) Robotics architecture of the mobile servicing system for the International Space Station. In: International Symposium on robotics, pp 416-421
5. Didot F, Oort M, Kouwen J, Verzijden P (2001) The era system: control architecture and performance results. In: Proc. 6th International Symposium on Artificial Intelligence, Robotics and Automation in Space (i-SAIRAS), Montral, Canada
6. Sato N, Doi S (2000) JEM Remote Manipulator System (JEMRMS) Human-In-the-Loop Test. In: International Symposium on Space Technology and Science, 22nd Japan, Morioka, pp 1195–1199
7. Yoshida K (2003) Engineering test satellite VII flight experiments for space robot dynamics and control: theories on laboratory test beds ten years ago, now in orbit. Int J Robot Res 22:321–335
8. Yoshida K, Nakanishi H, Inaba N, Ueno H, Oda M (2004) Contact dynamics and control strategy based on impedance matching for robotic capture of a non-cooperative satellite. In: Proc. 15th

CISM-IFToMM Symp. On Robot Design, Dynamics and Control-Romansy, St-Hubert, Canada
9. Yoshida K, Nakanishi H, Ueno H, Inaba N, Nishimaki T, Oda M (2004) Dynamics, control and impedance matching for robotic capture of a non-cooperative satellite. Adv Robot 18:175–198
10. Diftler M, Badger J, Joyce C, Potter E, Pike L (2015) Robonaut 2-building a robot on the international space station. In: ISS Research and Development Conference, 7–9 July 2015, Boston, MA, United States
11. Ceccarelli M, Li H, Carbone G, Huang Q (2015) Conceptual kinematic design and performance evaluation of a chameleon-like service robot for space stations. Int J Adv Robot Syst 12:17. doi:10.5772/60203
12. Bualat M, Barlow J, Fong T, Provencher C, Smith T, Zuniga A (2015) Astrobee: developing a free-flying robot for the international space station. In: AIAA SPACE 2014 Conference and Exposition, p 4643
13. Pardini C, Hanada T, Krisko PH (2009) Benefits and risks of using electrodynamic tethers to de-orbit spacecraft. Acta Astronaut 64:571–588
14. Williams P, Blanksby C, Trivailo P, Fujii HA (2005) In-plane payload capture using tethers. Acta Astronaut 57:772–787
15. Huang P, Wang D, Meng Z, Liu Z (2015) Post-capture attitude control for a tethered space robot-target combination system. Robotica 33:898–919
16. Michael N, Fink J, Kumar V (2011) Cooperative manipulation and transportation with aerial robots. Auton Robots 30:73–86
17. Michael N, Kim S, Fink J, Kumar V (2009) Kinematics and statics of cooperative multi-robot aerial manipulation with cables. In: ASME International Design Engineering Technical Conferences and Computers and Information in Engineering Conference 2009, pp 83–91
18. Cheng P, Fink J, Kumar V, Pang J-S (2009) Cooperative towing with multiple robots. J Mech Robot 1:011008
19. Bonometti J (2006) Boom rendezvous alternative docking approach. Space 19–21
20. Zhai G, Qiu Y, Liang B, Li C (2009) On-orbit capture with flexible tether-net system. Acta Astronaut 65:613–623
21. Huang P, Zhang F, Ma J, Meng Z, Liu Z (2015) Dynamics and configuration control of the maneuvering-net space robot system. Adv Space Res 55:1004–1014
22. Carricato M, Abbasnejad G (2013) Direct geometrico-static analysis of under-constrained cable-driven parallel robots with 4 cables. In: Bruckmann T, Pott A (eds) Cable-Driven Parallel Robots, Springer, pp 269–285
23. Riechel A, Bosscher P, Lipkin H, Ebert-Uphoff I (2004) Concept paper: cable-driven robots for use in hazardous environments. Inl Proceedings of the 10th international topical meeting on robotics and remote systems for hazardous environments
24. Rekleitis I, Martin E, Rouleau G, L'Archevêque R, Parsa K, Dupuis E (2007) Autonomous capture of a tumbling satellite. J Field Robot 24:275–296
25. Jasiobedski P, Greenspan M, Roth G (2001) Pose determination and tracking for autonomous satellite capture. In: 6th International Symposium on Artificial Intelligence, Robotics and Automation in Space. Montreal, Quebec, Canada. June 2001. NRC 45869
26. Matsumoto S, Jacobsen S, Dubowsky S, Ohkami Y (2003) Approach planning and guidance for uncontrolled rotating satellite capture considering collision avoidance. In: Proceedings of the 7th International Symposium on Artificial Intelligence and Robotics and Automation in Space: i-SAIRAS
27. Lim WB, Yang G, Yeo SH, Mustafa SK (2011) A generic force-closure analysis algorithm for cable-driven parallel manipulators. Mech Mach Theory 46:1265–1275